RESEARCH PAPER

Influence of nanotube physicochemical properties on the decoration of multiwall carbon nanotubes with magnetic particles

E. G. Uc-Cayetano · F. Avilés · J. V. Cauich-Rodríguez · R. Schönfelder ·
A. Bachmatiuk · M. H. Rümmeli · F. Rubio · M. P. Gutiérrez-Amador ·
G. J. Cruz

Abstract Two types of commercial multiwall carbon nanotubes (MWCNTs) with different diameters and physicochemical properties were decorated with iron oxide nanoparticles obtained by hydrolysis at high temperature in the presence of triethylene glycol and iron(III) chloride as metal precursor. A homogeneous distribution of 2–9 nm diameter particles decorating the MWCNTs was achieved using a weight concentration of 1:1 or 1:2 of the nanotube with respect to the metal precursor for 30 min of reflux. Detailed characterization of the as-received MWCNTs allowed to correlate the influence of the initial nanotube physicochemical properties to their decoration. The results indicate that a more homogeneous decoration and larger magnetization are achieved for MWCNTs with larger density of defective/reactive sites and larger surface area.

Keywords Carbon nanotubes · Oxidation · Decoration · Nanoparticles · Iron oxide · Nanocomposites

E. G. Uc-Cayetano (✉) · F. Avilés (✉) ·
J. V. Cauich-Rodríguez
Unidad de Materiales, Centro de Investigación Científica de Yucatán, A.C., Calle 43 # 130, Col. Chuburná de Hidalgo, 97200 Mérida, Yucatán, Mexico
e-mail: eguc_2909@hotmail.com

F. Avilés
e-mail: faviles@cicy.mx

R. Schönfelder · A. Bachmatiuk · M. H. Rümmeli
Dep. 11 (Electronic and Optical Properties) Molecular Nanostructures, Leibniz Institute for Solid State and Materials Research Dresden (IFW Dresden), Helmholtzstrasse 20, 01069 Dresden, Germany

M. H. Rümmeli
Department of Energy Science, Center for Integrated Nanostructure Physics, Institute for Basic Science, Sungkyunkwan University, Seoul, Republic of Korea

F. Rubio
Departamento de Química-Física de Superficies y Procesos, Instituto de Cerámica y Vidrio, CSIC, Campus de Cantoblanco. C/Kelsen, 5, 28049 Madrid, Spain

M. P. Gutiérrez-Amador
Escuela Superior de Apan, UAEH, Chimalpa Tlalayote, Municipio de Apan, Hidalgo, Mexico

G. J. Cruz
Departamento de Física, Instituto Nacional de Investigaciones Nucleares (ININ), Carretera México-Toluca s/n, CP 52750 La Marquesa Ocoyoacac, Mexico

Introduction

Decoration of multiwall carbon nanotubes (MWCNTs) consists of depositing nanoparticles on the MWCNT walls and/or ends, bonded by physical interactions (Lu 2007) with potential applications in catalysis, biosensors, biomedical, magnetic data storage, and electronic devices (Li et al. 2010; Wu et al. 2011; Liu et al. 2009a; Zhang et al. 2009). Methods proposed to achieve this goal include precipitation, hydrolysis at high temperature, or chemical decomposition of a metal precursor (Lu 2007; Huiqun et al. 2006; Liu et al. 2009b; Wan et al. 2007; Wang et al. 2009). A critical aspect of decoration with metallic particles is to achieve a homogeneous distribution of nanoparticles on the surface of MWCNTs. The type of metallic nanoparticle used for decoration can be diverse, and depending on the application varies from transition metals such as Co nanoparticles (Liu et al. 2009b), Ni (Liu et al. 2009b), Ru (Lu 2007) or Pd (Kuvarega et al. 2012) to noble metals such as Ag (Zamudio et al. 2006), Au (Hou et al. 2009) or Pt (Xing 2004). The use of iron oxide nanoparticles is common in the development of sensing, biological, electrical, and magnetic devices, due to their ferrimagnetic or superparamagnetic properties, which suggests their use as drug delivery systems, cell targeting, and different cancer therapies (Wu et al. 2011; Liu et al. 2009a, b; Zhang et al. 2009; Huiqun et al. 2006; Wan et al. 2007; Wang et al. 2009; Chu et al. 2013). Several studies on MWCNT decoration emphasize the need of initial surface modification through an oxidative treatment for the success of decoration (Lu 2007; Kardimi et al. 2012; Fan and Li 2012; Chopra et al. 2011). Although several methods have been proposed to decorate MWCNTs with magnetic iron oxide nanoparticles (Wu et al. 2011; Liu et al. 2009a, b; Zhang et al. 2009; Huiqun et al. 2006; Wan et al. 2007; Wang et al. 2009), it is not yet clear how the MWCNT morphology, initial structural ordering, and physicochemical properties influence their decoration, which is addressed here. The role of the concentration of the iron precursor and treatment time has also not been thoroughly investigated, and such a topic is also addressed herein.

In the present work, the use of an iron precursor to obtain decorated MWCNTs with magnetic properties for prospective applications in electrochemical biosensing is investigated. The main focus of the work is to evaluate the influence of two types of MWCNTs with different initial morphology and structural ordering on the decoration of MWCNTs with magnetic iron oxide nanoparticles.

Experimental

Materials

Two types of commercial MWCNTs were used in this research, which will be hereafter named "A" and "B" according to Table 1. Type "A" are <95 wt% pure MWCNTs (Baytubes C150P, Bayer MaterialScience AG, Leverkusen, Germany) with an outer diameter of 13–16 nm, inner diameter of 2–6 nm, and length ∼1–4 μm, according to the manufacturer. Type "B" are >95 wt% pure MWCNTs (Cheap Tubes Inc., Brattleboro, USA) with an outer diameter of 50–80 nm, inner diameter of 5–10 nm, and length of 10–20 μm. The BET surface area and Raman intensity ratio (I_G/I_D) included in Table 1 are outcomes of this research which will be discussed in the results section, and are included in advance for ease of the discussion. Sulfuric acid 98.6 % (v/v) and nitric acid 70 % (v/v) were purchased from J.T. Baker; triethylene glycol (TREG) 99 % v/v was purchased from Sigma-Aldrich, iron (III) chloride hexahydrate (99 %) and anhydrous sodium acetate (99 % w/w) were acquired from Merck.

MWCNT oxidation

MWCNTs were oxidized by an acid treatment before their decoration with iron oxide nanoparticles. The MWCNT oxidation used a liquid method based on a mixture of HNO_3 and H_2SO_4 as oxidizing agents which has shown its efficiency in the generation of OH, CO, and COOH functional groups on the surface of MWCNTs (Liu et al. 2009b; Fan and Li 2012; Chopra et al. 2011; Avilés et al. 2009; Wepasnick et al. 2011). This procedure consists of dispersing 0.3 g of MWCNTs in 70 ml of a mixture of 8.0 M HNO_3 (35 ml) and 8.0 M H_2SO_4 (35 ml), stirring for 15 min at 60 °C followed by 2 h of dispersion in an ultrasonic bath (100 W, 42 kHz) (Avilés et al. 2009). The treated MWCNTs are then washed with distilled water, filtered, and dried at 100 °C for 12 h.

MWCNT decoration

The method used for decorating MWCNTs with iron oxide nanoparticles consisted of dispersing 100 mg of

Table 1 Physical properties of the MWCNTs used

MWCNTs	Inner diameter (nm)	Outer diameter (nm)	Length (μm)	BET surface area (m^2/g)	Raman I_G/I_D
A	2–6	13–16	1–4	197	0.42 ± 0.01
B	5–10	50–80	10–20	110	0.89 ± 0.01

Table 2 Decorating treatments conducted on the MWCNTs and their identification according to the precursor concentration and nanotube type

MWCNT	A		B	
Weight ratio of MWCNTs: $FeCl_3 \cdot 6H_2O$	1:1	1:2	1:1	1:2
Identification	1:1-A	1:2-A	1:1-B	1:2-B

oxidized MWCNTs assisted by ultrasound in 50 ml of TREG for 1 h and adding the metal precursor in reflux at 200 °C. After dispersion, 100 mg (1:1) or 200 mg (1:2) of $FeCl_3 \cdot 6H_2O$ and 3.6 g of anhydrous sodium acetate were added to the solution. The resulting mixture was brought to reflux at 200 °C for 30 min. The obtained MWCNTs were then centrifuged with acetone, washed and filtered with distilled water, and finally dried at 100 °C for 12 h. Table 2 shows the decoration treatments discussed herein for the two types of oxidized MWCNTs investigated and the two final weight concentrations of metal precursor used. These two concentrations were selected based on preliminary analysis which evaluated different metal precursor concentrations and reflux times (see Table S1 in the supplementary material). As seen from the supplementary material, increasing the concentration of metal precursor or the reflux time with respect to those used in Table 2 yields a nonhomogeneous decoration.

Characterization of MWCNTs

As-received MWCNTs were characterized by Fourier transform infrared spectroscopy (FT-IR) using a Nicolet Protégé 460 equipment in a spectral range from 4,000 to 400 cm^{-1}. The samples were obtained from KBr pellets containing a small amount of MWCNTs. Raman spectroscopy was conducted with a Kaiser optical system and a helium–neon laser of 632 nm wavelength; the samples were prepared by dispersing 5 mg of MWCNTs into 10 ml of acetone by ultrasonic dispersion and drop-wise depositing the

MWCNT/acetone solution on an aluminum foil over a hot plate at 60 °C, allowing acetone to evaporate. Nitrogen adsorption–desorption isotherms at 77 K were measured using a Micromeritics TriStar 3000 equipment. Transmission electron microscopy (TEM) was carried out in a Jeol, JEM-2010F operated at 80 kV.

Decorated MWCNTs were characterized by TEM and Raman spectroscopy under conditions similar to the as-received MWCNTs. Energy dispersive X-ray (EDX) analysis was carried out in a Jeol SEM 6360LB microscope; X-ray powder diffraction (XRD) was carried out in a Siemens D5000 diffractometer at 40 kV, 20 mA, with a step time of 10 s and step angles of 0.02°; thermogravimetric analysis (TGA) was carried out using a Perkin Elmer Pyris 1 analyzer at a heating rate of 10 °C/min under synthetic air flow of 20 ml/min; X-ray photoelectron spectroscopy (XPS) was conducted with a Thermo K-Alpha spectrometer equipped with a monochromatic Al X-ray source (1486.6 eV) and spot size of 400 μm; the magnetic response of decorated MWCNTs was carried out in a vibrating sample magnetometer LDJ-9600 applying a maximum field of 15,000 Oe at room temperature.

Results and discussion

Characterization of as-received MWCNTs

Both as-received MWCNTs listed in Table 1 were first characterized in detail in order to investigate the influence of their initial properties on their decoration. Figure 1 shows representative FT-IR spectra of as-received MWCNTs of type A and B, where the labels "A" and "B" represent the nanotubes listed in Table 1. The FT-IR spectra were normalized to the band corresponding to conjugated C=C at $\sim 1,630$ cm^{-1}, in an attempt to assign meaningful conclusions to the changes in band intensities. As observed in Fig. 1, the absorption bands detected are similar for both as-received MWCNTs (A and B).
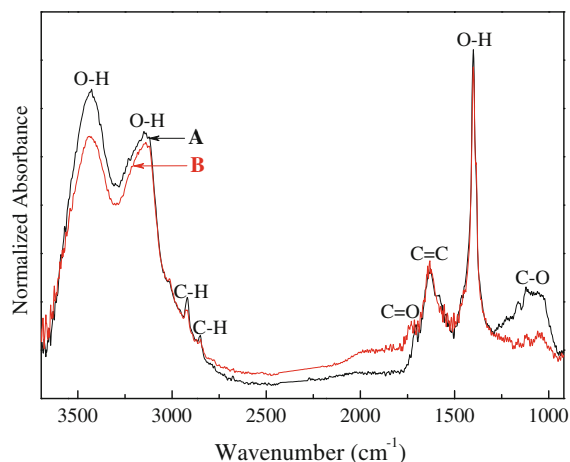
Fig. 1 FT-IR spectra of as-received MWCNTs. Labels *A* and *B* refer to Table 1

Both MWCNTs exhibited absorptions between 3,000–3,500 and ~1,400 cm^{-1}, indicating the presence of hydroxyl functional groups; bands at ~1,600 cm^{-1} were assigned to vibration of conjugated C=C, while at ~2,850 and ~2,920 cm^{-1} C–H stretching vibrations were observed (Avilés et al. 2009). Stretching vibration of carbonyl groups related to the presence of carboxylic acids was observed at ~1,720 cm^{-1} (Avilés et al. 2009), whereas the band at ~1,110 cm^{-1} was assigned to CO bonds (Wepasnick et al. 2011). The intensity of the band at ~1,110 cm^{-1} (CO) was slightly higher for MWCNTs of type A than those of type B. Therefore, the FT-IR analysis concludes that the MWCNTs already contain

a significant amount of functional groups from their synthesis and/or purification and that they are present in both as-received nanotubes in a similar fashion. However, the amount of oxygen-containing groups on nanotubes of type A may be slightly higher than those of type B.

Regarding the acid oxidation of the as-received MWCNTs, it has been previously shown that the acid oxidation conducted here increases the amount of oxygen-containing functional groups (Avilés et al. 2009; Wepasnick et al. 2011; Schönfelder et al. 2011).

Figure 2 shows TEM images of as-received MWCNTs of type A (a) and type B (b). The dimensions of both nanotubes reasonably agree with those provided by the manufacturer, which are listed in Table 1. For type A MWCNTs (Fig. 2a), structural damage is observed on the MWCNTs walls, in the form of a rough surface with significant kinks and bends along the MWCNT length. MWCNTs of type B (Fig. 2b) present similar kind of defects but apparently to a less extent.

It has been reported that the acidic oxidation conducted on the as-received MWCNTs herein slightly increases the density and extent of such structural defects on the MWCNT's surface (Avilés et al. 2012).

Figure 3 shows the complete range of partial pressure of N$_2$ adsorption–desorption isotherms of as-received MWCNTs. These isotherms can be identified as "Type IV" according to the IUPAC classification (Sing et al. 1985), corresponding to mesoporous materials with hysteresis loops occurring around $0.60 < P/P_0 < 1$. The BET specific areas (S_{BET}) were
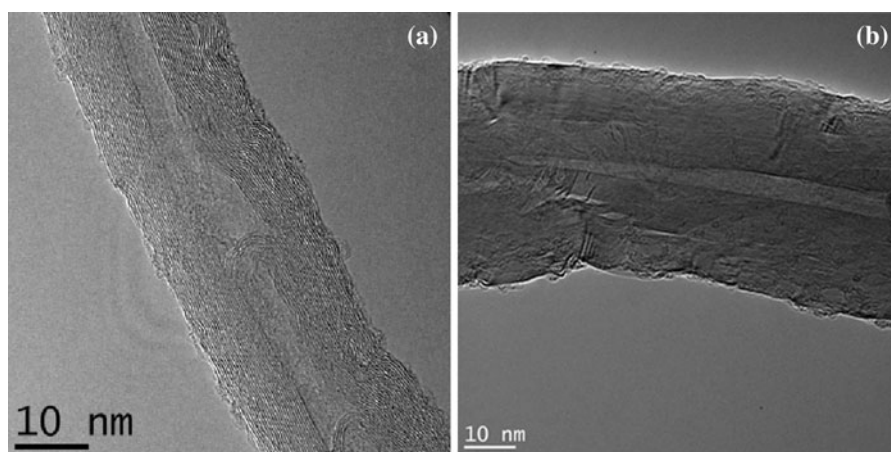

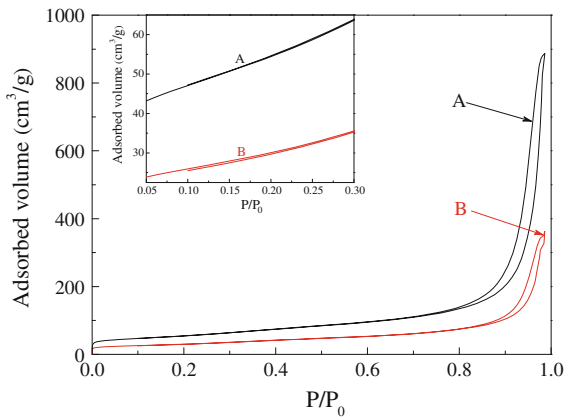**Fig. 2** TEM micrographs of as-received MWCNTs. **a** Type A, **b** type B

Fig. 3 N₂ adsorption–desorption isotherms for as-received MWCNTs. The *inset* shows the close-up of the interval $P/P_0 = 0.05$–0.30 used to calculate S_{BET}

determined using the Brunauer, Emmett, and Teller equation (Gregg and Sing 1982). The inset of Fig. 3 shows a magnification of the interval $P/P_0 = 0.05$–0.30 used for S_{BET} calculation. The BET specific areas obtained were $S_{BET} = 197$ m²/g for MWCNTs type A and $S_{BET} = 110$ m²/g for MWCNTs type B (listed in Table 1, "Materials" section), which correlate well with the rougher and more irregular surface observed by TEM. It has been shown that acid oxidation generates more surface defects, eliminates surface traces of amorphous carbon, and hence increases the S_{BET} surface area (Aviles et al. 2013).

Figure 4 shows representative Raman spectra of both types of as-received MWCNTs investigated. The G band is a first-order Raman mode located around 1,580–1,600 cm⁻¹ and corresponds to vibrations of sp² carbon atoms. The D band originates from a second-order scattering process which occurs around 1,280–1,350 cm⁻¹ and represents loss of translational symmetry in the network and provides information about the presence of vacancies, defects, and the finite size of the network (Dresselhaus et al. 2010).

To characterize the structural ordering of the MWCNTs, the intensity ratio between the G and D bands (I_G/I_D) can be used (Dresselhaus et al. 2010, 2005; Antunes et al. 2006). This strategy was used here followed by band deconvolution, and the results are presented in Table 3.

The G and D bands observed in Fig. 4a, b are broad, which is a characteristic feature of commercial MWCNTs (Dresselhaus et al. 2010, 2005). For MWCNTs, the apparent broad shape of the G band is often convoluted and composed of two main bands, the G one itself located at or close to 1,585 cm⁻¹ and a second band called D′ located around 1,620 cm⁻¹ (Dresselhaus et al. 2010, 2005; Antunes et al. 2006). The D and D′ bands are explained by the double resonance theory and are related to structural defects. In double resonance processes, the origin of the D and D′ bands and many weak dispersive phonon modes in the Raman spectra of graphite are explained by resonant enhancement of Raman intensity in two
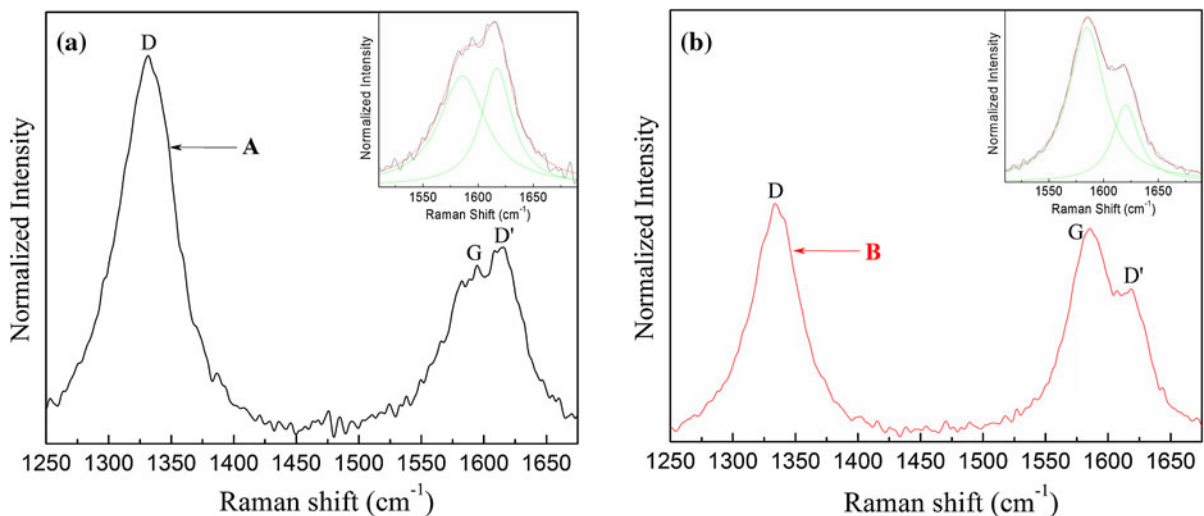

Fig. 4 Raman spectra of as-received MWCNTs. **a** Type A, **b** type B. *Inset* Deconvolution of the G band

Table 3 Features of the Raman spectra of as-received MWCNTs and deconvolution of the band at $\sim 1{,}600$ cm^{-1}

MWCNTs	Raman shift (cm^{-1})			FWHM (cm^{-1})			I_G/I_D ratio	$I_G/I_{D'}$ ratio
	G band	D band	D$'$ band	G band	D band	D$'$ band		
A	1586	1331	1617	51.0 ± 0.1	$57.0 + 0.3$	$33.7 + 0.01$	$0.42 + 0.01$	$0.90 + 0.01$
B	1585	1334	1620	40.3 ± 0.04	$47.7 + 0.2$	$28.9 + 0.03$	$0.89 + 0.01$	$1.43 + 0.01$

consecutive scattering processes (Antunes et al. 2006). The shape of the band located between 1,550 and 1,650 cm^{-1} is quite different for MWCNTs of type A or B, which was very reproducible in several samples analyzed. The wide band around 1,620 cm^{-1} corresponding to D' is clearly more intense for MWCNTs type A than those of type B, but is convoluted with the G band. Therefore, this wide band was deconvoluted using Lorentzian shapes for G and D', and the deconvoluted bands are shown as insets in Fig. 4a, b. As can be seen from Table 3, the wide band centered around 1,600 cm^{-1} is deconvoluted into two bands centered around 1,585 cm^{-1} (G) and 1,620 cm^{-1} (D') for both types of MWCNTs. Analysis of the full-width-at-half-maximum (FWHM) also indicates that the G and D bands are significantly wider for MWCNTs of type A, which points out to larger structural disorder for these MWCNTs (Dillon et al. 2004). For MWCNTs of type A $I_G/I_D = 0.42$ and $I_G/I_{D'} = 0.90$, while for those of type B $I_G/I_D = 0.89$ and $I_G/I_{D'} = 1.43$. The reduced value of I_G/I_D and $I_G/I_{D'}$ (increased intensities of the D and D' bands) as well as the higher values of FWHM for MWCNTs of type A with respect to those of type B are a clear indication that the structural ordering is significantly less for MWCNTs of type A. Thus, a larger density of defects is present in MWCNTs of type A, and they may also perform as reactive sites for nanoparticle decoration.

No further significant changes in the Raman spectra of as-received MWCNTs were found after the oxidation treatment and after their decoration with iron oxide nanoparticles, and thus Raman spectra are not further discussed.

Characterization of decorated MWCNTs

Transmission electron microscopy

The influence of the concentration of the metal precursor and reflux time were first studied, and the results are discussed in the supplementary material. Initially, the weight ratio between MWCNTs and metal precursor was varied between 1:1 and 1:4, and the reaction (reflux) time was varied between 30 and 120 min. TEM analysis of the decorated MWCNTs showed that precursor concentrations higher than 1:2 and reflux times longer than 30 min rendered agglomerations of the iron oxide nanoparticles and/or inhomogeneous decoration (see Fig. S1 of supplementary material). Therefore, only the results for 1:1 and 1:2 precursor concentrations at 30 min of reflux time are discussed herein.

Figure 5 shows low and high magnification TEM images of both types of decorated MWCNTs at 1:1 and 1:2 concentrations of metal precursor and 30 min reflux time. The diameter of the decorating nanoparticles was measured from several images, and the histogram of their diameter distribution is shown in the last column of such a figure.

MWCNTs decorated with iron oxide nanoparticles attached to the MWCNT's outer walls are observed in Fig. 5 for both types of MWCNTs and decoration treatments (see Table 2). Attachment of iron oxide nanoparticles to the MWCNT walls is achieved by physical bonds and electrostatic attractions (Lu 2007). The mechanism for the decoration of nanotubes with iron oxide nanoparticles is based on the high temperature decomposition of iron(III) chloride hexahydrate in the form of iron oxides, which nucleate on the surface of the MWCNTs and provide a template for nanoparticle growth. The negatively charged functional groups on the oxidized MWCNT surface provide active sites for physical interactions with metallic ions (Liu et al. 2009a, b; Zhang et al. 2009).

Figure 5 shows that type A MWCNTs treated with a concentration of precursor of 1:2 present a large density of nanoparticles covering the MWCNTs and a homogenous distribution of iron nanoparticles on the MWCNT walls. Furthermore, the decorating particles do not concentrate only on individual nanotubes but

Fig. 5 TEM images and diameter distributions of decorated MWCNTs (A and B) for two concentrations of precursor (1:1 and 1:2). Treatment ID corresponds to those of Table 2

Treatment ID	Groups of MWCNTs	Individual MWCNTs	Diameter distribution
1:2-A			
1:1-A			
1:2-B			
1:1-B			
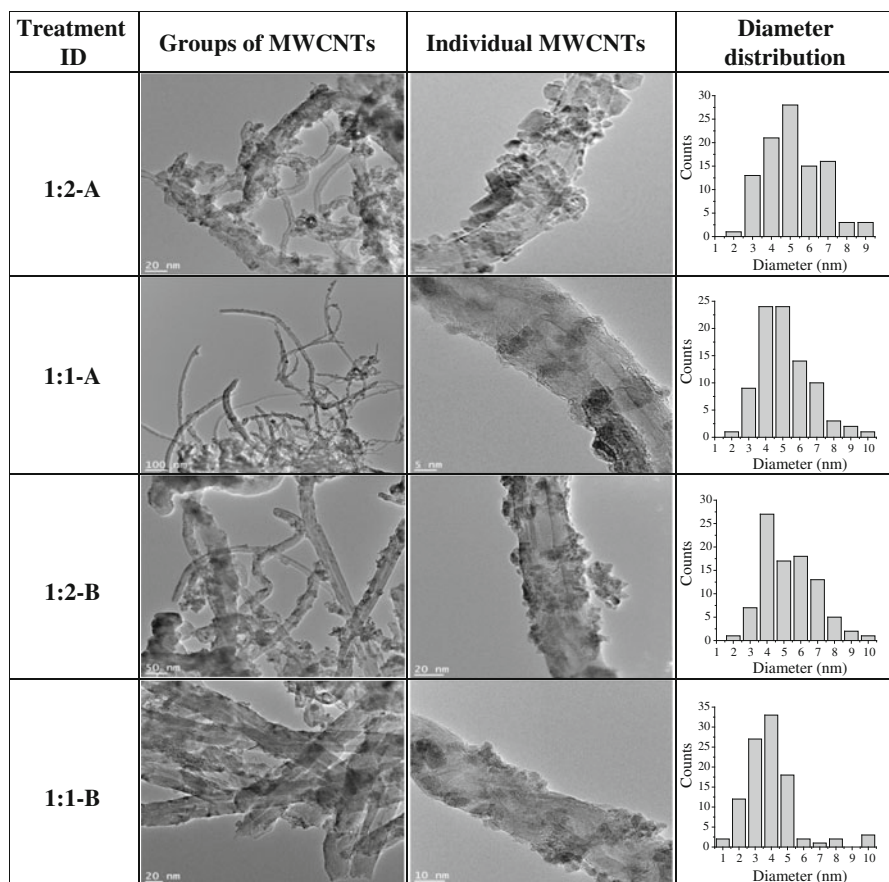
are well distributed over the treated MWCNTs, as shown by the TEM images capturing groups of decorated MWCNTs. The diameter of the decorating particles ranges from 2 to 9 nm for treatment 1:2-A, with a characteristic particle diameter of ~ 5 nm. For the treatment 1:1-A (decreased concentration of iron precursor for the same type of MWCNT), a homogeneous distribution of particles is also observed on the MWCNT walls, although the density of particles per nanotube surface area is slightly reduced. Similar trends are observed for type B MWCNTs treated with precursor concentrations of 1:2 (1:2-B) and 1:1 (1:1-B). However, a larger density of particles per nanotube with a more homogeneous distribution of decorating nanoparticle is observed for nanotubes of type A with respect to those of type B. Further increase in the precursor concentration and/or reaction time produced particle agglomeration and largely heterogeneous distribution of iron oxide particles over the MWCNTs (see supplementary material).

Energy dispersive X-ray analysis

Elemental analysis of decorated MWCNTs was obtained by EDX. The major elements present in the decorated samples are carbon, oxygen, and iron. Treatment 1:2 showed similar amounts of carbon ~ 60–63 wt%, oxygen ~ 18 wt%, and iron ~ 18–21 wt% for both types of MWCNTs (A and B), but there was a reduction in the amount of Fe (~ 12 wt%) when the precursor concentration was reduced to 1:1. The iron present in the sample could arise from element Fe or iron oxides. The amount of oxygen content in the decorated MWCNTs increased by ~ 10 wt% with respect to the oxidized samples, which suggests the formation of iron oxides.

X-ray powder diffraction

Figure 6 presents the diffraction patterns of both types of oxidized MWCNTs (Fig. 6a, b). Both MWCNTs show diffraction peaks at angles $2\theta = 26.6°$ and $43.5°$
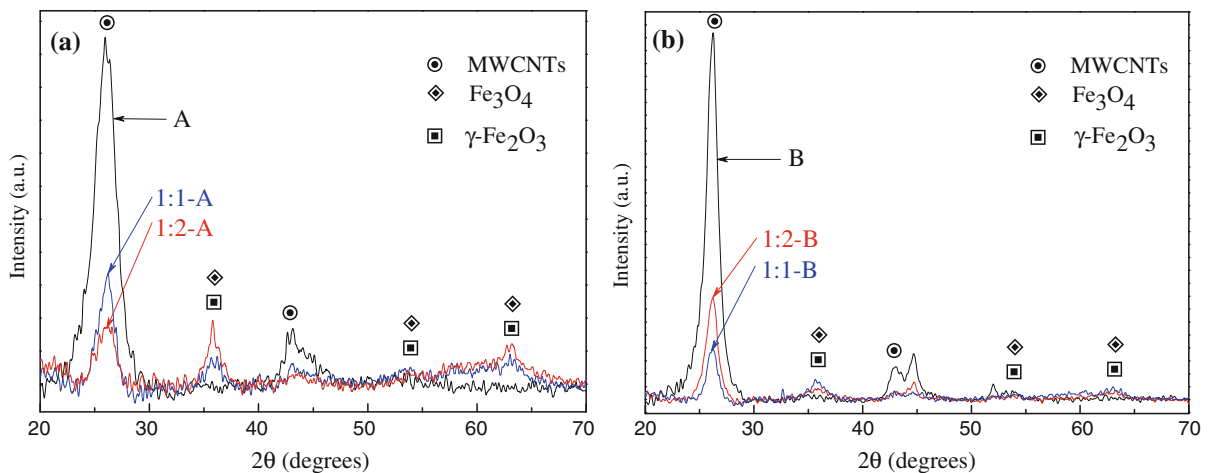
Fig. 6 XRD patterns of oxidized only (*black*) and decorated MWCNTs with two weight concentrations of metal precursor. **a** MWCNTs type A, **b** MWCNTs type B

which are attributed to the (002) and (100) planes of the MWCNTs, respectively (Zhang et al. 2005). These diffraction peaks are still present in the decorated MWCNTs, but new 2θ diffraction angles indicate the presence of iron oxide particles (Jiang et al. 2011). Decorated MWCNTs of type A exhibit new diffraction peaks at $2\theta = 35.5°$, $54.0°$, and $63.0°$, which correspond to the (311), (422), and (400) planes of magnetite (Fe_3O_4) but also overlap with some peaks of maghemite ($\gamma\text{-}Fe_2O_3$), according to the joint committee on powder diffraction standard (JCPDS) cards No. 19-629 for magnetite (Fe_3O_4) and No. 39-1346 for maghemite ($\gamma\text{-}Fe_2O_3$). Decorated MWCNTs of type B exhibit similar diffraction peaks at $2\theta = 35.5°$, $54.0°$, and $63.0°$, which suggest the coexistence of Fe_3O_4 and $\gamma\text{-}Fe_2O_3$ phases in both decorated samples. The intensity of the peaks corresponding to the iron oxide particles in decorated MWCNTs is different when comparing the ratio of intensities of the Fe_3O_4 principal diffraction peak at $2\theta = 35.5°$ ($I_{35.5°}$) to the diffraction peak of the carbon nanotube at $2\theta = 26.6°$ ($I_{26.6°}$). For MWCNTs of type A, the ratio $I_{26.6°}/I_{35.5°}$ is 0.91, while for MWCNTs of type B $I_{26.6°}/I_{35.5°}$ is 8.74. This clearly shows that the intensity of the iron oxide diffraction peak of decorated MWCNTs 1:2-A is higher than that of 1:2-B, which consistently points to a larger density of decorating nanoparticles per unit nanotube surface area for MWCNTs with more defective sites (i.e., type A).

Thermogravimetric analysis

Figure 7 shows thermogravimetric analyses under synthetic air flow of both types of oxidized and decorated MWCNTs with different weight concentration of precursor (1:1 and 1:2). The weight losses before ~150 °C are associated to evaporation of physisorbed water and possible decomposition of a few oxygen-containing groups. Dehydration and decarboxylation of functional groups are expected to occur between 150 and 350 °C for MWCNTs without decoration (Wepasnick et al. 2011; Rosario-Castro et al. 2009). However, for decorated MWCNTs, the iron oxide nanoparticles catalyze the thermal degradation of both amorphous carbon and the carbon nanostructure itself (Wepasnick et al. 2011; Rosario-Castro et al. 2009; Zhao et al. 2012) producing a marked weight loss in the 200–300 °C region. The steeper degradation for concentration 1:2 with respect to 1:1 indicates a higher density of decorating particles for 1:2. After this zone, thermal degradation of the graphitic structure (sp^2) of the nanotube occurs, which also occurs at lower temperatures for decorated nanotubes. The maximum rate of weight loss and the temperature at which this fastest decomposition occurs (T_d) can be identified by the derivative of the TGA curve (inset in Fig. 7). For MWCNTs of type A, T_d of the samples that were only oxidized was ~621 °C, corresponding to the oxidation of the graphitic structure of the MWCNTs; however, for
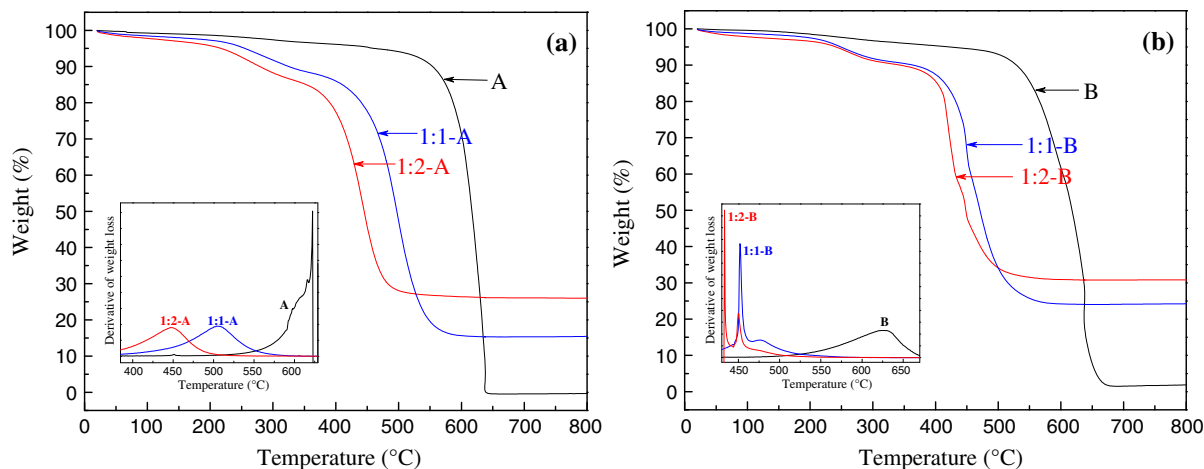
Fig. 7 TGA of oxidized and decorated MWCNTs with different weight concentrations. **a** MWCNTs type A, **b** MWCNTs type B

the decorated MWCNTs of type A with a precursor concentration of 1:1 and 1:2, T_d was ~ 505 and ~ 448 °C, respectively. For the MWCNTs of type B, T_d of the oxidized samples was ~ 626 °C, while that of the decorated samples with a precursor concentration of 1:1 and 1:2 was 451 and 476 °C, respectively. The higher thermal stability of MWCNTs type B (without decoration) with respect to those of type A correlates well with their less defective structure quantified by Raman spectroscopy. The lower T_d for decorated samples confirms the enhanced oxidation activity of the iron oxide nanoparticles (Wepasnick et al. 2011; Rosario-Castro et al. 2009; Zhao et al. 2012; Kauffman et al. 2010). The fact that the decomposition occurs at lower temperatures for concentrations 1:2 with respect to 1:1, specially for MWCNTs of type A (see insets in Fig. 7), indicates a larger amount of iron oxide nanoparticles for such a concentration.

The remaining weight of both types of the MWCNTs after 650 °C provides valuable information about the amount of iron oxide particles in the decorated samples. While both MWCNTs without decoration lose all their mass at ~ 650 °C, both types of decorated MWCNTs at precursor concentration of 1:2 retain ~ 30 wt% after all the carbon material is burned off. Treatment 1:1 exhibits a slight reduction in the weight retained after 600 °C yielding ~ 20–25 wt%, in agreement with the EDX results. The majority of this weight percentage should correspond to the weight of iron oxide nanoparticles decorating the MWCNTs, since the metallic impurities

already present in the MWCNTs before decoration are <1 wt%. Under conditions of high temperature and air atmosphere, Fe_3O_4 may easily turn into Fe_2O_3.

X-ray photoelectron spectroscopy

Figure 8 shows XPS spectra of decorated MWCNTs (A and B) prepared with different weight concentrations of precursor (1:1 and 1:2). The XPS survey of both decorated MWCNTs (Fig. 8a, c) show bands at ~ 285, 532, and 711 eV which are attributed to the energetic distribution of C 1s, O 1s, and Fe 2p orbitals of Fe_3O_4, respectively (Liu et al. 2009a; Fan and Li 2012; Han et al. 2012). Fe $2p_{1/2}$ and Fe $2p_{3/2}$ bands located at 711 and 724.9 eV are related to Fe chemical states in Fe_3O_4 (Missana et al. 2003; Torres Sanchez et al. 1990; Jiang et al. 2011), and the orbital between Fe $2p_{1/2}$ and Fe $2p_{3/2}$ (insets in Fig. 8a, c) suggests that additional Fe states could be found in the γ-Fe_2O_3 form (Kauffman et al. 2010; Han et al. 2012; Jiang et al. 2011). There is also a shift from 532 to 530 eV and widening of the O 1s band for the decorated samples (Fig. 8b, d), which was further analyzed by band deconvolution using Lorentzian curves (see deconvolution inset in Fig. 8b, d). Three bands are present in the deconvolution spectra of O 1s (inset in Fig. 8b, d), which correspond to C=O at 532.8 eV, C–O–H at 531.3 eV, and Fe–O–Fe at 530.2 eV (Han et al. 2012). The FWHM of those bands are 2.29 eV (C=O), 1.50 eV (C–O–H), and 0.99 eV (Fe–O–Fe) for MWCNTs of type A and 2.13 eV (C=O), 1.50 eV (C–
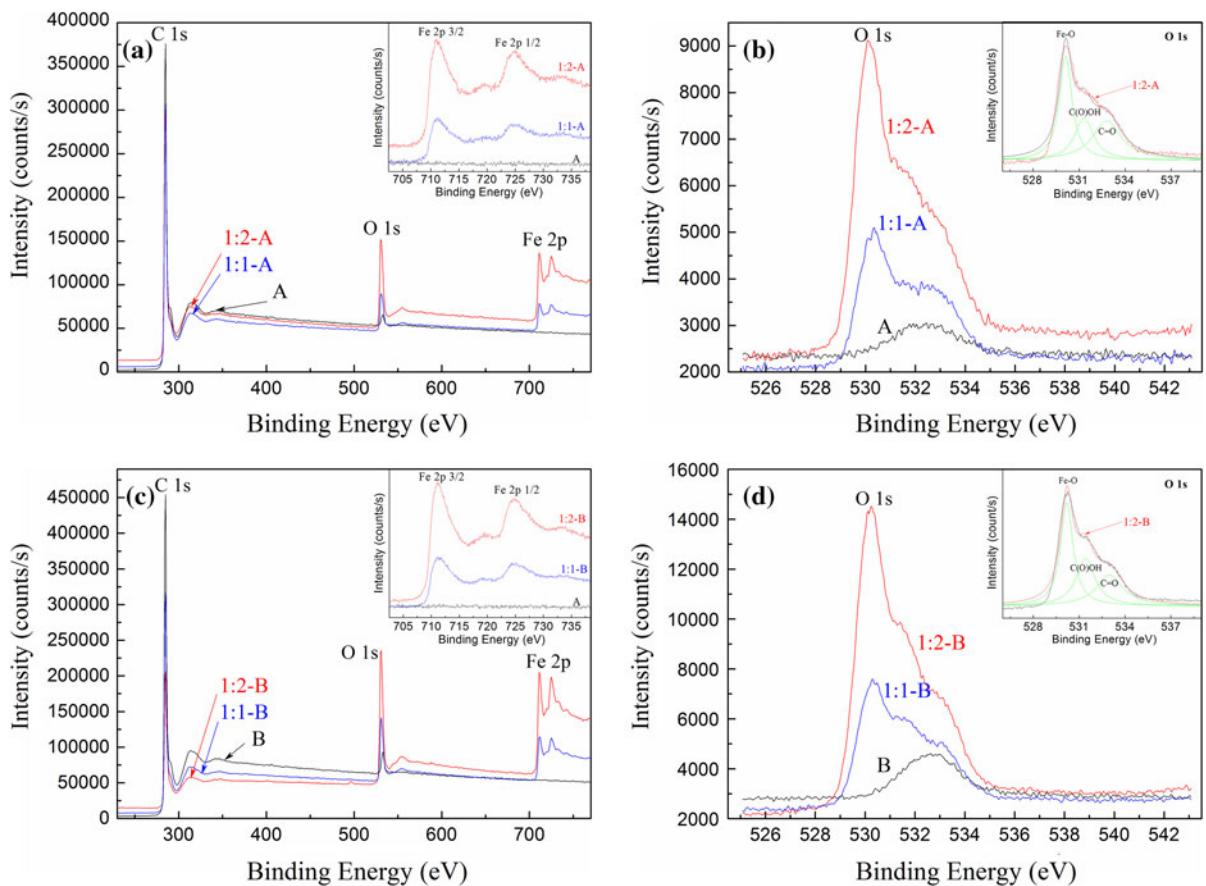
Fig. 8 XPS spectrum of decorated MWCNTs (A and B) with different weight concentration of precursor (1:1 and 1:2). **a** Survey for MWCNTs type A, **b** O 1s orbitals for MWCNTs type A, **c** survey for MWCNTs type B, **d** O 1s orbitals for MWCNTs type B. *Insets* of **a** and **c** are the Fe 2p orbitals and of **b** and **d** are the deconvolution of the O 1s band

O–H), and 0.98 eV (Fe–O–Fe) for MWCNTs of type B. These functional bands can be related to the contribution of oxygen in Fe_3O_4 [33, Han et al. 2012]. The ratio between the XPS intensities of Fe–O–Fe (530.2 eV) and C–O–H (531.3 eV) in MWCNTs of type A ($I_{Fe–O–Fe}/I_{C–O–H}$) is ∼2.5, while for MWCNTs of type B $I_{Fe–O–Fe}/I_{C–O–H}$ is ∼2.2. The difference between these intensity ratios consistently suggests that a larger density of Fe_3O_4 nanoparticles is found in MWCNTs of type A. Therefore, the XPS analysis consistently indicates that magnetite (Fe_3O_4) is the dominant phase present in the decorating nanoparticles, which coexists with maghemite (γ-Fe_2O_3). The ratio of intensities in the deconvolution analysis also suggests that a higher density of decorating nanoparticles is present on the MWCNTs of type A compared to those of type B, consistently with the XRD and TGA analyses.

Vibrating magnetometry

A simple magnetic experiment (see Fig. S2 in supplementary material) proved that all decorated MWCNTs investigated herein are attracted by a small commercial magnet of 0.4 T. In order to quantify this magnetic behavior, Fig. 9 shows the magnetic hysteresis loops of both types of decorated MWCNTs obtained using vibrating sample magnetometry. For MWCNTs of type A, the saturation magnetization for 1:1-A and 1:2-A decorated samples are ∼1.7 and ∼5.6 emu/g, respectively, with coercive fields of 90.9 Oe (1:1-A) and 92.9 Oe (1:2-A). For MWCNTs of type B, the saturation magnetization is ∼2 emu/g with coercive field of 179.5 Oe for treatment 1:1-B and ∼4.3 emu/g with a coercive field of 161.5 Oe for treatment 1:2-B. Albeit small, the hysteresis in the curves is non-zero; so, the behavior can be classified as ferrimagnetic. The
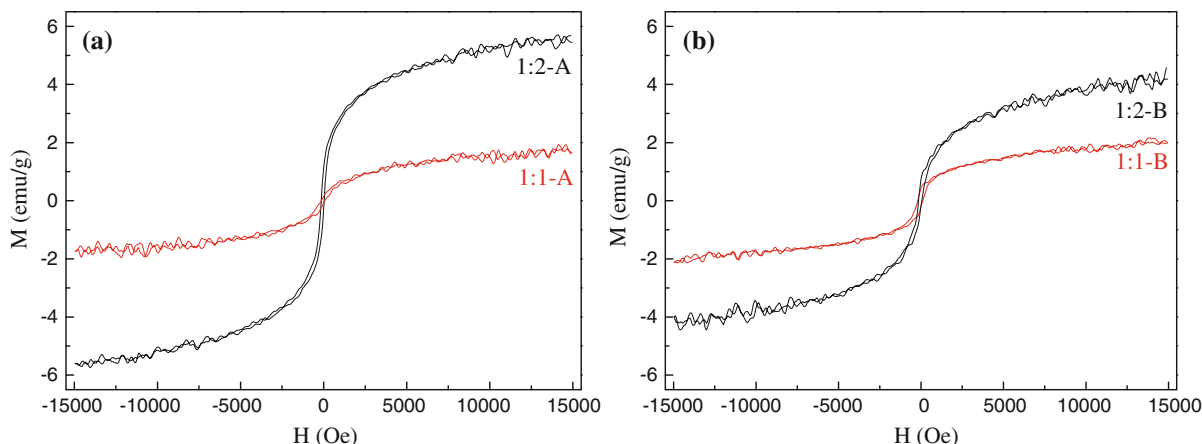
Fig. 9 Magnetization curves of decorated MWCNTs with two precursor concentrations (1:1 and 1:2). **a** MWCNTs of type A, **b** MWCNTs of type B

relatively low values of saturation magnetization further support the presence of maghemite. At the precursor concentration of 1:1, both decorated MWCNTs have similar values of saturation magnetization, but for treatments with precursor concentration of 1:2, the saturation values are higher for MWCNTs type A than for type B. The differences in saturation magnetizations values may be attributed to the differences in the Fe_3O_4 degree of coverage on the MWCNTs, dispersion, and particle size (Wan et al. 2007; Fan and Li 2012; Gao et al. 2009).

Discussion

The various characterization techniques used here have shown that a higher density of well-distributed decorating particles is found in MWCNTs of type A with respect to MWCNTs of type B (see Table 1 for the description of both MWCNTs). This can be explained by the larger amount of defective/reactive sites of MWCNTs type A, quantified by the I_G/I_D and $I_G/I_{D'}$ ratios of their Raman spectra. The deconvolution of the Raman spectra into these bands proved that the structural ordering is very different between both as-received MWCNTs. The BET surface area is also higher for MWCNTs of type A, and its diameter is smaller than those of MWCNTs of type B, which may also be contributing factors.

Quantum mechanics simulations using density functional theory (DFT) to study the adsorption of single

metallic atoms on defective carbon nanotubes (such as those containing vacancies) indicate that the stronger binding energy at the MWCNTs defect sites enhances nanoparticle adsorption on MWCNT sites with a high density of defects (Park et al. 2007). DFT calculations reveal that the interactions between functionalized carbon nanotubes and iron oxide particles are enhanced by carbon defects such as vacancies (Yin et al. 2011).

For the MWCNTs used in this investigation, Raman spectroscopy proved the existence of a larger density of initial defective sites for those of type "A". These defective sites act as reactive sites for iron oxide nanoparticle bonding, and the density of the functional groups of such defective sites is expected to be extended after the acid oxidation treatment. The increased substrate surface area available also influences the MWCNT decoration. Therefore, MWCNTs with larger number of defective sites and larger surface area (labeled "A" herein) are more suitable for decoration.

Conclusions

MWCNTs were decorated with magnetic iron oxide nanoparticles with a characteristic diameter of 5 nm, which render the nanotube a low hysteretic ferrimagnetic behavior. EDX and TGA indicate that the weight content of iron oxide nanoparticles present on the surface of the MWCNTs is around 20–30 % (depending on the precursor concentration). XRD and XPS

showed that the decorating particles are magnetite (Fe_3O_4) coexisting with maghemite (γ-Fe_2O_3). The results obtained from the decoration of MWCNTs with magnetic iron oxide nanoparticles show that a homogeneous decoration with nanoparticles of ~ 5 nm diameter can be achieved for 1:1 and 1:2 weight concentrations of metal precursor (MWCNTs: precursor) employing 30 min as reaction time. Defective sites on the MWCNT walls play a prominent role for MWCNT decoration with iron oxide nanoparticles, acting as reactive sites for decoration. MWCNTs with higher density of defective sites and larger surface area render a higher density of decoration and larger magnetization values.

References

Antunes EF, Lobo AO, Corat EJ, Trava-Airoldi VJ, Martin AA, Veríssimo C (2006) Comparative study of first- and second-order Raman spectra of MWCNT at visible and infrared laser excitation. Carbon 44:2202–2211

Aviles F, Sierra-Chi CA, Nistal A, May-Pat A, Rubio F, Rubio J (2013) Influence of silane concentration on the functionalization of multiwall carbon nanotubes. Carbon 57:520–529

Avilés F, Cauich-Rodríguez JV, Moo-Tah L, May-Pat A, Vargas-Coronado R (2009) Evaluation of mild acid oxidation treatments for MWCNT functionalization. Carbon 47:2970–2975

Avilés F, Ponce A, Cauich-Rodriguez JV, Martínez GT (2012) TEM observations of MWCNTs oxidized by mild experimental conditions. Fuller Nanotube Car N 20:49–55

Chopra N, McWhinney HG, Shi W (2011) Chemical changes in carbon nanotube-nickel/nickel oxide core/shell nanoparticle heterostructures treated at high temperatures. Mater Charact 62:635–641

Chu M, Shao Y, Peng J, Dai X, Li H, Wu Q, Shi D (2013) Near-infrared laser light mediated cancer therapy by photothermal effect of Fe_3O_4 magnetic nanoparticles. Biomaterials 34:4078–4088

Dillon AC, Yudasaka M, Dresselhaus MS (2004) Employing Raman spectroscopy to qualitatively evaluate the purity of carbon single-wall nanotube materials. J Nanosci Nanotechnol 4:691–703

Dresselhaus MS, Dresselhaus G, Saito R, Jorio A (2005) Raman spectroscopy of carbon nanotubes. Phys Rep 409:47–99

Dresselhaus MS, Jorio A, Souza Filho AG, Saito R (2010) Defect characterization in graphene and carbon. Phil Trans R Soc A 368:5355–5377

Fan XJ, Li X (2012) Preparation and magnetic property of multiwalled carbon nanotubes decorated by Fe_3O_4 nanoparticles. New Carbon Mater 27–2:111–116

Gao Q, Chen F, Zhang J, Hong G, Ni J, Wei X, Wang D (2009) The study of novel Fe_3O_4@γ-Fe_2O_3 core/shell nanomaterials with improved properties. J Magn Magn Mater 321:1052–1057

Gregg SJ, Sing KSW (1982) Adsorption, surface area and porosity. Academic Press, London

Han Q, Wang Z, Xia J, Chen S, Zhang X, Ding M (2012) Facile and tunable fabrication of Fe_3O_4/graphene oxide nanocomposites and their application in the magnetic solid-phase extraction of polycyclic aromatic hydrocarbons from environmental water samples. Talanta 101:388–395

Hou X, Wang L, Zhou F, Wang F (2009) High-density attachment of gold nanoparticles on functionalized multiwalled carbon nanotubes using ion exchange. Carbon 47:1209–1213

Huiqun C, Meifang Z, Yaogang L (2006) Decoration of carbon nanotubes with iron oxide. J Solid State Chem 179:1208–1213

Jiang W, Lai KL, Hu H, Zeng XB, Lan F, Liu KX, Wu Y, Gu ZW (2011) The effect of $[Fe^{3+}]/[Fe^{2+}]$ molar ratio and iron salts concentration on the properties of superparamagnetic iron oxide nanoparticles in the water/ethanol/toluene system. J Nanopart Res 13:5135–5145

Kardimi K, Tsoufis T, Tomou A, Kooi BJ, Prodromidis M, Gournis D (2012) Synthesis and characterization of carbon nanotubes decorated with Pt and PtRu nanoparticles and assessment of their electrocatalytic performance. Int J Hydrogen Energy 37:1243–1253

Kauffman DR, Sorescu DC, Schofield DP, Allen BL, Jordan KD, Star A (2010) Understanding the sensor response of metal decorated carbon nanotubes. Nano Lett 10:958–963

Kuvarega AT, Krause RWM, Mamba BB (2012) Multiwalled carbon nanotubes decorated with nitrogen, palladium co-doped TiO_2 (MWCNT/N, Pd co-doped TiO_2) for visible light photocatalytic degradation of Eosin Yellow in water. J Nanopart Res 14:776–792

Li J, Yuan R, Chai Y, Che X (2010) Fabrication of a novel glucose biosensor based on Pt nanoparticles-decorated iron oxide-multiwall carbon nanotubes magnetic composite. J Mol Catal B 66:8–14

Liu Y, Jiang W, Li S, Cheng ZP, Song D, Zhang XJ, Li FS (2009a) Attachment of magnetic nanoparticles on carbon nanotubes using oleate as an interlinker molecule. Mater Chem Phys 116:438–441

Liu Y, Jiang W, Xu L, Yang X, Li F (2009b) Decoration of carbon nanotubes with nearly monodisperse MIIFe$_2$O$_4$ (MFe_2O_4, M = Fe, Co, Ni) nanoparticles. Mater Lett 63:2526–2528

Lu J (2007) Effect of surface modifications on the decoration of multi-walled carbon nanotubes with ruthenium nanoparticles. Carbon 45:1599–1605

Missana T, Maffiotte C, García-Gutiérrez M (2003) Surface reactions kinetics between nanocrystalline magnetite and uranyl. J Colloid Interf Sci 261:154–160

Park Y, Lahaye RJWE, Lee YH (2007) Adsorption of Pt on defective carbon nanotube walls: a DFT approach. Comput Phys Commun 177:46

Rosario-Castro BI, Contés EJ, Lebrón-Colón M, Meador MA, Sánchez-Pomales G, Cabrera CR (2009) Combined electron microscopy and spectroscopy characterization of as-received, acid purified, and oxidized HiPCO single-wall carbon nanotubes. Mater Charact 60:1442–1453

Schönfelder R, Avilés F, Bachmatiuk A, Cauich-Rodriguez JV, Knupfer M, Büchner B, Rümeli MH (2011) On the merits of Raman spectroscopy and thermogravimetric analysis to asses carbon nanotube structural modifications. Appl Phys A 106:843–852

Sing KSW, Everett DH, Haul RAW, Moscou L, Pierotti RA, Rouquérol J (1985) Reporting physisorption data for gas/solid systems. International union of pure and applied chemistry (IUPAC). Pure Appl Chem 57:603–619

Torres Sanchez RM, Curt EM, Volzone C, Mercader RC, Cavalieri AL (1990) Study of Fe(II) oxidation in ground magnetite. Mater Res Bull 25:553–561

Wan J, Cai W, Feng J, Meng X, Liu E (2007) In situ decoration of carbon nanotubes with nearly monodisperse magnetite nanoparticles in liquid polyols. J Mater Chem 17:1188–1192

Wang H, Cao L, Yan S, Huang N, Xiao Z (2009) An efficient method for decoration of the MWCNTs with nearly monodispersed magnetite nanoparticles. Mat Sci Eng B 164:191–194

Wepasnick KA, Smith BA, Schrote KE, Wilson HK, Diegelmann SR, Fairbrother DH (2011) Surface and structural characterization of multi-walled carbon nanotubes following different oxidative treatments. Carbon 49:24–36

Wu H, Liu G, Zhuang Y, Wu D, Zhang H, Yang H, Hu H, Yang S (2011) The behavior after intravenous injection in mice of multiwalled carbon nanotube/Fe$_3$O$_4$ hybrid MRI contrast agents. Biomaterials 32:4867–4876

Xing Y (2004) Synthesis and electrochemical characterization of uniformly-dispersed high loading Pt nanoparticles on sonochemically-treated carbon nanotubes. J Phys Chem B 108:19255–19259

Yin WJ, Wei SH, Ban C, Wu Z, Al-Jassim MM, Yan Y (2011) Origin of bonding between the SWCNT and the Fe$_3$O$_4$ (001) surface and the enhanced electrical conductivity. J. Phys Chem Lett 2:2853–2858

Zamudio A, Elas AL, Rodríguez-Manzo JA, López-Uras F, Rodríguez-Gattorno G, Lupo F, Rühle M, Smith DJ, Terrones H, Díaz D, Terrones M (2006) Efficient anchoring of silver nanoparticles on N-doped carbon nanotubes. Small 2:346–350

Zhang D, Shi L, Fang J, Dai K (2005) Preparation and modification of carbon nanotubes. Mater Lett 59:4044–4047

Zhang Q, Zhu M, Zhang Q, Li Y, Wang H (2009) Synthesis and characterization of carbon nanotubes decorated with manganese–zinc ferrite nanospheres. Mater Chem Phys 116:658–662

Zhao F, Duan H, Wang W, Wang J (2012) Synthesis and characterization of magnetic Fe/CNTs composites with controllable Fe nanoparticle concentration. Physica B 407:2495–2499